THE JOURNAL OF PHYSICAL CHEMISTRY Letters

Letter

Cite This: J. Phys. Chem. Lett. 2019, 10, 3756−3762

pubs.acs.org/JPCL

Bandlike Transport in PbS Quantum Dot Superlattices with Quantum Confinement

Yun Liu,[†] Nolan Peard,[‡] and Jeffrey C. Grossman*[,†]

[†]Department of Materials Science and Engineering, Massachusetts Institute of Technology, Cambridge, Massachusetts 02139, United States

[‡]Department of Physics, Massachusetts Institute of Technology, Cambridge, Massachusetts 02139, United States

Supporting Information

ABSTRACT: Optoelectronic devices made from colloidal quantum dots (CQDs) often take advantage of the combination of tunable quantum-confined optical properties and carrier mobilities of strongly coupled systems. In this work, first-principles calculations are applied to investigate the electronic, optical, and transport properties of PbS CQD superlattices. Our results show that even in the regime of strong necking and fusing between PbS CQDs, quantum confinement can be generally preserved. In particular, computed carrier mobilities for simple cubic and two-dimensional square lattices fused along the {100} facets are 2−3 orders of magnitude larger than those of superlattices fused along {110} and {111} facets. The relative magnitude of the electron and hole mobilities strongly depends on the crystal and electronic structures. Our results illustrate the importance of understanding the crystal structure of CQD films and that strongly fused CQD superlattices offer a promising pathway for achieving tunable quantum-confined optical properties while increasing carrier mobilities.

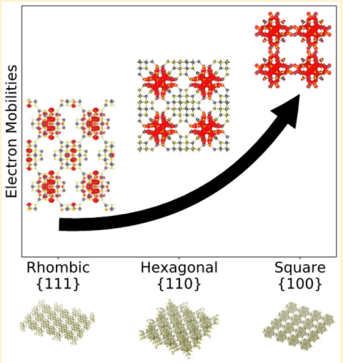

Colloidal semiconductor quantum dots (CQDs) have attracted a significant amount of attention due to their size- and ligand-tunable electronic properties and facile synthesis in solution. Their versatility is attractive for a wide range of applications such as light-emitting diodes,[1,2] photodetectors,[3,4] and solar cells.[5,6] In particular, PbS is one of the best performing quantum dot photovoltaic (PV) materials with a certified solar conversion efficiency of >11%.[7] Carrier mobility is one of the most important parameters for PV devices and plays an important role in controlling the device short-circuit current and fill factor.[8] Since the first report of charge carrier communication between CQDs in solids,[9] improved size control, ligand chemistry, and device fabrication techniques have enhanced carrier mobilities from 10^{-3}−10^{-2} to 24 $cm^2 V^{-1} s^{-1}$.[10,11] It has also been shown that carrier mobilities increase exponentially with decreasing ligand length,[12] and the new classes of atomic and short organic ligands also allowed improvements in band alignment, absorption coefficients, and PV efficiencies.[6,13,14] To achieve enhanced connectivity between dots, CQDs can be fused directly with one another.[15] The orientation, degree of fusing, and morphology of the fused CQDs can be controlled by varying the synthesis conditions,[16] suggesting that strongly fused CQDs could provide a pathway for resolving the two seemingly contradictory requirements for future optoelectronics: tunable quantum-confined optical properties and strong electronic coupling.[17,18]

In addition to fusing CQDs, many recent efforts have focused on synthesizing highly monodisperse CQD superlattice films with improved size and energy level homogeneity.[7,19] For example, Weidman et al. synthesized highly monodisperse PbS films by self-assembly, characterizing a transformation from face-centered cubic (FCC) to body-centered cubic (BCC) configurations.[20,21] Through nanocrystal attachment control, superlattices in both two-dimensional (2D) square and honeycomb lattices have been achieved for PbSe CQDs.[22] Binary, ternary, and quaternary superlattices have also been assembled for improved functionalities by combining the photoluminescent, plasmonic, and magnetic properties of each nanocrystal component.[23,24] On the theoretical front, Kalesaki et al. investigated the electronic structures of 2D CdSe and PbSe honeycomb and square superlattices using a tight-binding approach[25,26] and demonstrated the existence of nontrivial flat bands, Dirac cones, and topological edge states. While hopping transport is the dominant charge transport mechanism in colloidal nanocrystals,[27−29] there have been reports of bandlike transport in coherent CdSe[30,31] and PbSe[32] thin films with electron mobilities approaching those of their bulk counterparts. In this Letter, we use density functional theory (DFT) calculations and the Boltzmann transport equation to investigate the effects of crystal structure and fusing orientation on the electronic, optical, and bandlike transport properties of PbS CQD superlattices.

To model the CQD superlattices in the strong fusing regime, we ignored ligands in our calculations. Direct fusing between CQD where the ligands were stripped has been observed and

Received: May 5, 2019
Accepted: June 12, 2019
Published: June 12, 2019

DOI: 10.1021/acs.jpclett.9b01282
J. Phys. Chem. Lett. 2019, 10, 3756−3762

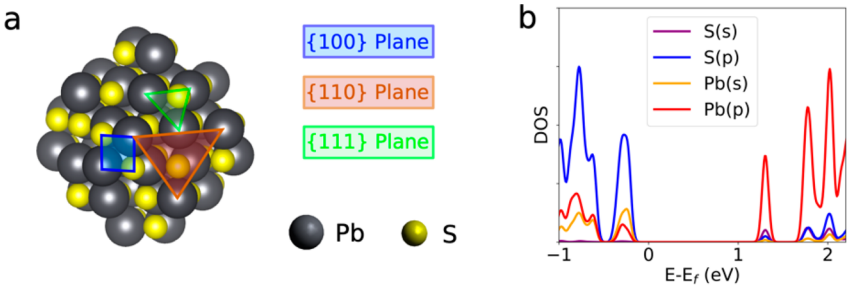

Figure 1. (a) Prototype $Pb_{44}S_{44}$ nanocrystal with a diameter of 1.5 nm and its lattice planes. (b) PDOS showing that the HOMO and LUMO are predominantly S 3(p) and Pb 6(p) characteristics.

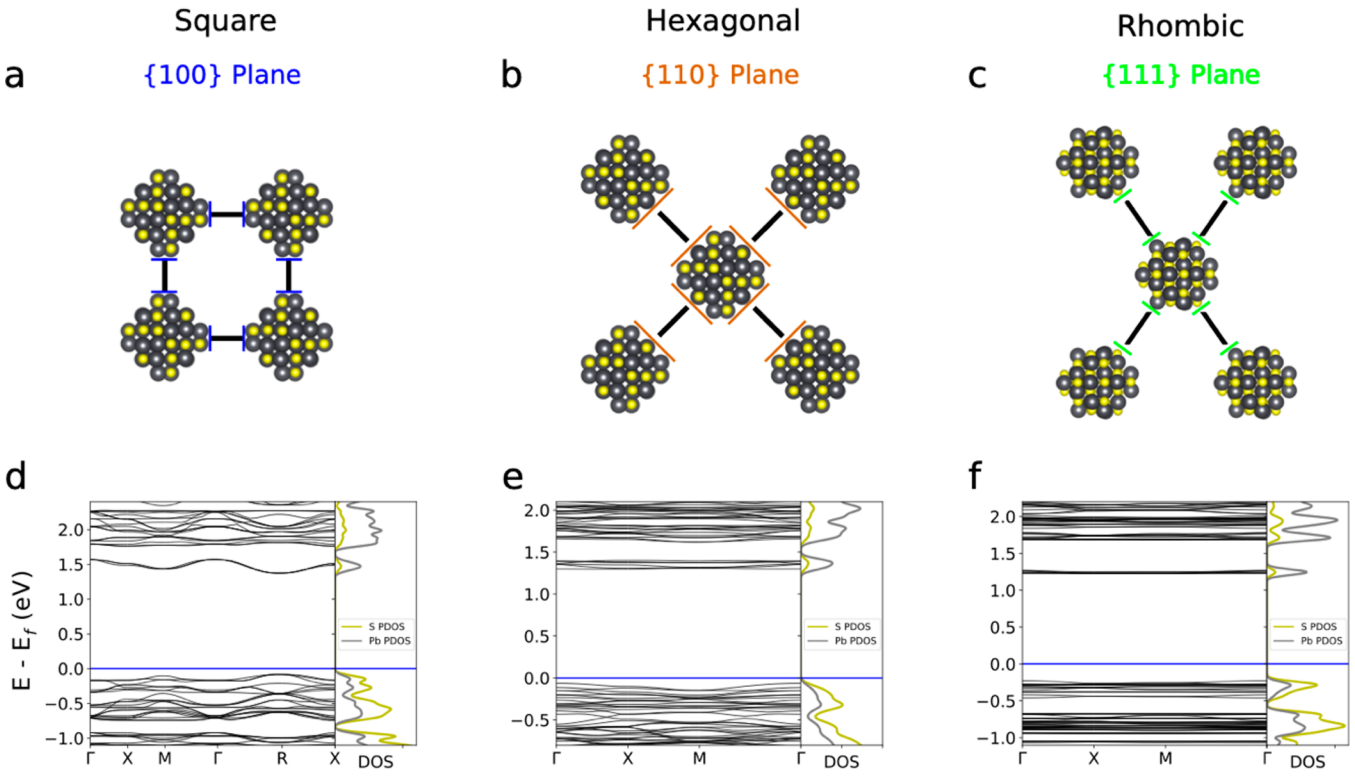

Figure 2. Schematics showing the crystal structure of the nanocrystal arranged in 2D (a) square, (b) hexagonal, and (c) rhombic superlattices connected via {100}, {110}, and {111} facets, respectively, viewed from the *z*-axis. Their corresponding band structure and PDOS are shown in panels d–f, respectively. The bandgap is at (d) $M = [1/2, 1/2, 0]$, (e) $\Gamma = [0, 0, 0]$, and (f) $\Gamma = [0, 0, 0]$. All energies are referenced to the Fermi level indicated by the blue line.

engineered on purpose in experiments,[15,16] and this approach allows us to explore the upper bound of carrier mobilities in highly fused CQDs. A bare PbS nanocrystal with a diameter of ∼1.5 nm and a calculated gap between the highest occupied molecular orbital (HOMO) and the lowest unoccupied molecular orbital (LUMO) of 1.4 eV was used to create 2D and three-dimensional (3D) superlattices, as shown in Figure 1. The occupied orbitals and unoccupied orbitals near the Fermi level mainly consists of S(p) and Pb(p) orbital contributions, respectively.[33] (Figure 1b). The large energy splitting between the LUMO and LUMO+1 states is due to the loss of translational symmetry in the nanocrystal.[34]

2D Superlattice. First, we considered 2D square, hexagonal, and rhombic superlattices formed by necking CQDs via the {100}, {110}, and {111} planes (Figure 2). The band structure and partial DOS (PDOS) of the superlattices show that the contributions of orbitals near the Fermi level are similar to that of the isolated CQD. A distinct first excitation peak for each superlattice exists in the optical spectra shown in Figure 3a, indicating that quantum confinement is preserved. These peaks

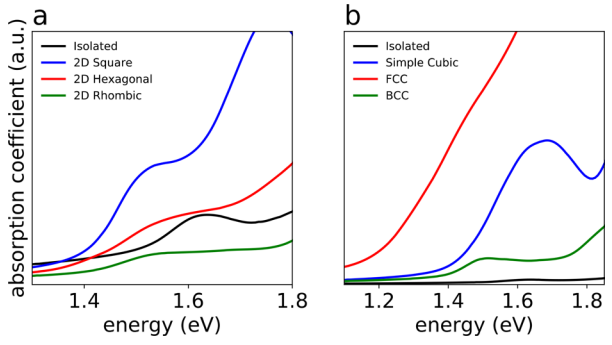

Figure 3. Absorption spectra of (a) 2D superlattices and (b) 3D superlattices compared with those of a single isolated quantum dot.

DOI: 10.1021/acs.jpclett.9b01282
J. Phys. Chem. Lett. 2019, 10, 3756−3762

Table 1. Calculated Electron and Hole Mobilities for 2D and 3D Superlattices

	2D rhombic	2D hexagonal	2D square	BCC	SC ($Pb_{44}S_{44}$)	SC ($Pb_{140}S_{140}$)	experiments
electron mobility ($cm^2\ V^{-1}\ s^{-1}$)	6.4×10^{-5} (x) 9.0×10^{-5} (y)	4.8×10^{-5}	1.5×10^{-3}	8.4×10^{-6}	7.9×10^{-3}	1.1×10^{-2}	~10^{-4} to 10^{-1}[42−45]
hole mobility ($cm^2\ V^{-1}\ s^{-1}$)	1.2×10^{-5} (x) 2.8×10^{-5} (y)	5.6×10^{-4}	1.1×10^{-3}	4.5×10^{-5}	3.9×10^{-2}	7.4×10^{-2}	~10^{-4} to 10^{-3}[42−45]

are red-shifted by ~0.1 eV compared with the first excitation peak of the isolated CQD, due to moderate delocalization of the wave function into neighboring CQDs.

We next calculated carrier mobilities using the effective mass approximation and deformation potential theory.[35] We tested the validity of the method for the bulk PbS solid, which has well-reported electron (μ_e) and hole mobilities (μ_h) of 600 and 540 cm V^{-1} s^{-1}, respectively, at 300 K. Using the elastic modulus and effective masses reported in the literature[36−39] and computed deformation potentials of 22 and 56 eV for electrons and holes, we obtained a μ_e of 9.30×10^3 $cm^2\ V^{-1}\ s^{-1}$ and a μ_h of 1.20×10^3 $cm^2\ V^{-1}\ s^{-1}$ (for details, see the Supporting Information). The overestimation by theory mainly arises from the fact that deformation potential takes into account only intravalley acoustic phonon scattering, while in polar materials such as PbS, there is significant scattering of carriers by optical phonons, which decreases the carrier mobilities.[40]

Hybrid functionals and spin−orbit coupling (SOC) corrections are necessary to accurately describe the electronic structures of the lead chalcogenide family of semiconductors.[36,38] Using a semilocal functional such as PBE and neglecting SOC effects would overestimate the effective masses, resulting in a μ_e of 120 $cm^2\ V^{-1}\ s^{-1}$ and a μ_h of 150 $cm^2\ V^{-1}\ s^{-1}$. These values are slightly lower but on the same order of magnitude as the experimental values. These results taken together suggest that error cancellations arising from (1) neglecting optical phonon scattering and (2) neglecting SOC and using the PBE functional are why our computed mobilities are in good agreement with experiments. Despite these opposing errors, we remain confident that the trends computed are representative because the errors on the different superlattices are comparable to each other.

The computed electron and hole mobilities of the square lattice are ~2 orders of magnitude higher than those of hexagonal and rhombic lattices (Table 1). Because the HOMO and LUMO of single CQD have a small contribution from {100} facets but no contributions from {110} and {111} facets,[15,41] there is a much stronger wave function overlap between CQDs connected via {100} facets (Figure 4).

For PbS CQDs, μ_e is larger than μ_h due to the greater spatial delocalization of the single dot LUMO compared to that of the HOMO.[8,15] On the other hand, μ_e is lower than μ_h in bulk PbS as the hole effective mass m^*_h is smaller than the electron effective mass m^*_e.[38,46] In our strongly coupled superlattices, the relative magnitudes of μ_e and μ_h change with their electronic structures. For example, μ_e is larger in the square lattice due to the greater degree of delocalization of the CBM states compared to that of the VBM states, similar to the isolated CQD case. For hexagonal lattices, however, the CBM wave function of one CQD is completely out of phase with its nearest neighbor, where coupling occurs only between second nearest neighbors (Figure 4d). The VBM states, on the other hand, are coupled between nearest neighbors (Figure 4c).

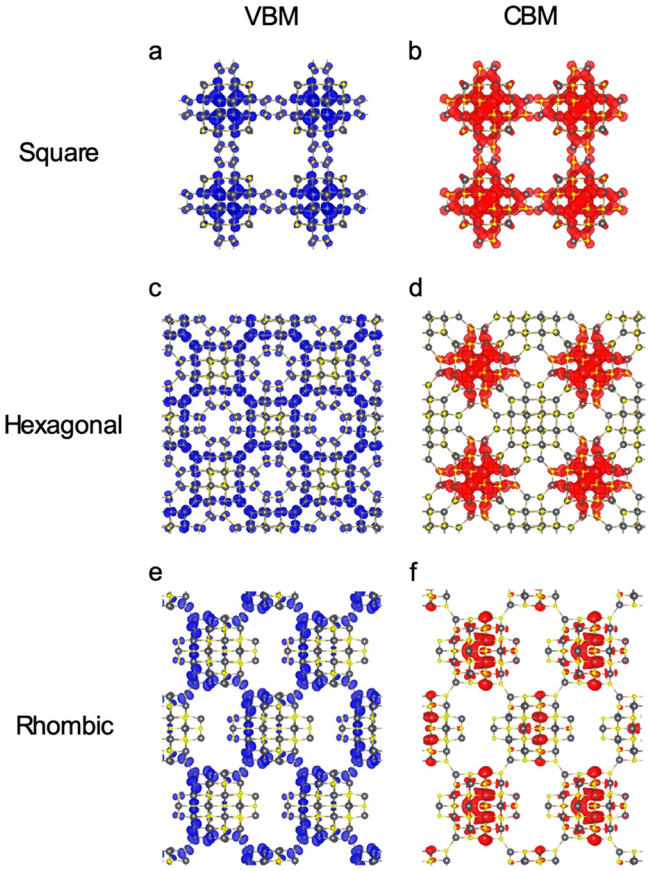

Figure 4. VBM and CBM of (a and b) the 2D square lattice at M = [1/2, 1/2, 0], (c and d) the 2D hexagonal lattice at Γ = [0, 0, 0], and (e and f) the 2D rhombic lattice at Γ = [0, 0, 0].

Therefore, m^*_h is smaller than m^*_e, with μ_e being smaller than μ_h by ~1 order of magnitude.

3D Superlattice. Due to its rock-salt crystal structure, the PbS nanocrystal is a truncated octahedron with 6 {100}, 8 {111}, and 12 {110} facets.[47−49] They then naturally form the 3D simple cubic (SC), BCC, and FCC superlattices with 6, 8, and 12 nearest neighbors (Figure S1). As we are in the high fusing regime, nanocrystals in the FCC lattice fused unintentionally along the {100} plane in addition to the {110} plane due to the shape of the nanocrystal, resulting in a high packing density approaching that of the bulk crystal. Quantum confinement is therefore lost in the FCC lattice with no observable excitation peak (Figure 3b), and we will not consider this case for transport calculations. In the intermediate fusing regime, we expect the presence of ligands will keep the CQDs farther apart and prevent such unintentional fusing. In contrast, quantum confinement is still preserved in the SC and BCC lattices. Similar to the case for the 2D superlattices, the carrier mobilities of the SC lattice connected via {100} planes are 3 orders of magnitude higher than those of the BCC lattice connected via {111} planes (Table 1), with similar wave

DOI: 10.1021/acs.jpclett.9b01282
J. Phys. Chem. Lett. 2019, 10, 3756−3762

function characteristics compared to the 2D counterparts (Figure S2). This shows that the connecting facets determine the fundamental coupling strength between CQDs.

There have been debates in the literature about how the carrier mobilities vary with CQD sizes. In the hopping regime, it was suggested that mobilities increase with CQD size because the number of hops needed for carriers to travel between the electrodes is reduced.[12] The activation energy for hopping also decreases with nanocrystal size, resulting in higher carrier mobilities.[50] On the other hand, as the size of the CQD increases, wave function overlap between CQDs decreases, resulting in lower carrier mobilities.[51] Often the competition between these factors makes it difficult to succinctly describe size-dependent trends.[52]

Here we investigated the size dependence of carrier mobilities in the bandlike regime. A larger prototype PbS nanocrystal model 2 nm in diameter ($Pb_{140}S_{140}$) is used to construct a SC lattice. Its electronic structure is shown in Figure S3, and quantum confinement is also preserved as seen in the optical spectra (Figure S4). Compared to the 1.5 nm CQD, $Pb_{140}S_{140}$ has lower effective masses (Table S1) due to the enhanced interdot coupling (Figure S3b). The effect is particularly significant for the CBM states, because a highly delocalized wave function is formed on the fused {100} plane (Figure S3c). The carrier mobilities increased by ∼100%. If we keep the number of fused atoms in the plane the same as that of $Pb_{44}S_{44}$, while increasing the CQD size, the couplings between neighboring CQDs are significantly reduced (Figure S3e,f); the carrier mobilities are then reduced by as much as 5 orders of magnitude with a μ_e of 4.5×10^{-8} cm^2 V^{-1} s^{-1} and a μ_h of 2.1×10^{-4} cm^2 V^{-1} s^{-1}. This nanocrystal model ($Pb_{92}S_{92}$), however, is unrealistic due to the large Wulff ratio (h_{111}/h_{100}).[41]

Our results show that in general the carrier mobilities increase with the size of the nanocrystals. This is due to the fact that as the radius of the nanocrystal (r) increases, the average distance between them increases linearly with r, decreasing the wave function overlap. The area of the connecting facet, however, increases as r^2, resulting in more atoms being in contact with each other and increasing the overall wave function overlap. However, the shape of the nanocrystal can change the wave function in a very drastic way, changing the carrier mobilities much more significantly.

We note that our calculated carrier mobilities should be interpreted qualitatively. Because we considered only superlattices in the strong fusing regime, ligands have been ignored. For CQD films with a low to moderate degree of fusing, the impact of ligands on the electronic, optical, and transport properties of superlattices should be systematically studied in further works. We also note that the prototype CQD model is small compared to those typically used in experiments, whose Wulff shape might vary due to changes in the surface energy. However, projection of the wave function onto the different planes in our small dots is qualitatively similar to that of larger dots studied previously.[33,41] Therefore, we believe these trends observed in our calculations to be useful. By varying the crystal structures, lattice dimensions, and size of CQDs, we can change the bandlike carrier mobilities by up to 4 orders of magnitude. In addition to the common crystal structure studied here, additional exotic crystal structures such as honeycomb lattice[53] provide a rich parameter space to explore to uncover the desired properties of CQD solids.

On the basis of our observations, we propose several design guidelines to achieve high mobilities in the PbS CQD superlattice. (1) If the CQD can be epitaxially aligned in a lattice, then simple cubic and square lattices that fuse along the {100} facet would represent the most promising choice. (2) If only the fusing facets can be controlled but not the crystal symmetry, our results suggest that the synthesis should maximize the number of {100} contacts between CQDs. (3) If the size of the CQD can be easily controlled, then the largest CQD with quantum-confined excitons (<18 nm) would be desirable.

In summary, our work shows that controlling the superlattice structures is crucial to manipulating the electronic, optical, and transport properties of highly fused PbS CQD solids. We showed that the quantum confinement of CQD solids is generally preserved even in the extreme fusing regime. Carrier mobilities of SC and square lattice connected via {100} facets are 2−3 orders of magnitude larger than those superlattices fused along {110} and {111} facets. The relative magnitude of electron and hole mobilities can also be manipulated through crystal structure engineering. Our results illustrate the importance of understanding the effects of crystal structure and connectivity of CQD films for improved optoelectronic performances and demonstrate that strongly fused CQD superlattices offer a promising pathway to having tunable quantum-confined optical properties while maintaining strong electronic coupling.

■ COMPUTATIONAL METHODS

All DFT calculations were performed using the Vienna Ab initio Simulation Package (VASP, version 5.4).[54,55] Electronic wave functions were expanded in a plane wave basis with an energy cutoff of 400 eV, and the core−valence interaction was treated by the projector-augmented wave (PAW) method.[56] Atomic positions were relaxed until the residual forces were <0.01 eV/Å. For all calculations, the Pb $5d^{10}6s^26p^2$ and S $3s^23p^6$ electrons were included in the valence and the exchange correlation functional was approximated by the Perdew−Burke−Ernzerhof (PBE) generalized gradient approximation.[57] A vacuum spacing of 15 Å was added to the supercell in the z-dimension to remove any spurious interactions in all 2D superlattices and in all three spatial dimensions for isolated nanocrystals.

The frequency-dependent dielectric function was computed using the independent particle approximation. The absorption coefficient, $\alpha(\omega)$, was obtained using the formula $\alpha(\omega) = \frac{\omega}{cn(\omega)}\varepsilon_2(\omega)$, where c is the speed of light in vacuum, $\varepsilon_2(\omega)$ is the imaginary part of the dielectric function, and $n(\omega)$ is the real part of the complex refractive index, $n^2(\omega) = \frac{1}{2}(\varepsilon_1 + \sqrt{\varepsilon_2^2 + \varepsilon_1^2})$, with $\varepsilon_1(\omega)$ being the real part of the dielectric function.

The electron and hole effective masses of the superlattices, m^*_e and m^*_h, respectively, were obtained from the energy bands of DFT calculations using the BoltzTraP code,[58] by taking the harmonic average of the parallel and perpendicular effective mass at the CBM and VBM states.[39] We increased Monkhorst−Pack Γ-centered k-point sampling for Brillouin zone integration until the effective masses were converged to $<0.1m_e$, where m_e is the rest mass of the electron. For 2D superlattices, only a single k-point is used in the z-direction.

DOI: 10.1021/acs.jpclett.9b01282
J. Phys. Chem. Lett. 2019, 10, 3756−3762

Elastic constant c_α for a 3D crystal is obtained by fitting the total energy change per volume ($\Delta E/V_0$) to dilation $(\Delta l/l_0)^2$ in the α direction, where V_0 and l_0 are the equilibrium volume and lattice constant, respectively. In two dimensions, the fitting is done using the energy change per area of the supercell ($\Delta E/S_0$) to dilation $(\Delta l/l_0)^2$. The deformation potential constants, D_α, for electrons and holes are obtained by fitting the energy change at either the conduction band minimum (CBM) or valence band minimum (VBM), Δe, to the lattice dilation $D_\alpha = \Delta e/(\Delta l/l_0)$ in the α direction.

The carrier mobilities in two and three dimensions can be computed using the following formula using the effective mass approximation to the Boltzmann transport equation and deformation potential theory

$$\mu_{2D} = \frac{2e_0\hbar^3 c_\alpha}{3D_\alpha^2 k_b T (m^*)^2}$$

$$\mu_{3D} = \frac{2(2\pi)^{1/2} e_0 \hbar^4 c_\alpha}{3D_\alpha^2 (k_b T)^{3/2} (m^*)^{5/2}}$$

where e_0 is the elementary charge, $\hbar$ is the reduced Planck constant, and k_b is the Boltzmann constant.

■ ASSOCIATED CONTENT

Supporting Information

The Supporting Information is available free of charge on the ACS Publications website at DOI: 10.1021/acs.jpclett.9b01282.

Calculations showing the estimate for the carrier mobilities of bulk PbS solid using effective mass approximation and deformation potential, figures showing crystal and electronic structure and wave functions of 3D superlattices, figures showing the electronic structure, VBM and CBM wave functions, and optical spectra of larger CQDs, and a table showing the effective masses, deformation potentials, and elastic constants of electrons and holes for all of the superlattices (PDF)

■ AUTHOR INFORMATION

Corresponding Author

*E-mail: jcg@mit.edu.

ORCID

Yun Liu: 0000-0003-1630-4052

Jeffrey C. Grossman: 0000-0003-1281-2359

Notes

The authors declare no competing financial interest.

■ ACKNOWLEDGMENTS

Y.L. is grateful for the support from a Singapore National Science Scholarship and the Tata GridEdge Program at the Massachusetts Institute of Technology. This research used the computational resources of the National Energy Research Scientific Computing Center, a U.S. Department of Energy (DOE) Office of Science User Facility supported by the Office of Science of the DOE under Contract DE-AC02-05CH11231, and the Extreme Science and Engineering Discovery Environment (XSEDE), which is supported by National Science Foundation Grant ACI-1053575.

■ REFERENCES

(1) Colvin, V. L.; Schlamp, M. C.; Alivisatos, a P. Light-Emitting-Diodes Made from Cadmium Selenide Nanocrystals and a Semiconducting Polymer. *Nature* **1994**, *370*, 354−357.

(2) Shirasaki, Y.; Supran, G. J.; Bawendi, M. G.; Bulović, V. Emergence of Colloidal Quantum-Dot Light-Emitting Technologies. *Nat. Photonics* **2013**, *7*, 13−23.

(3) Konstantatos, G.; Howard, I.; Fischer, A.; Hoogland, S.; Clifford, J.; Klem, E.; Levina, L.; Sargent, E. H. Ultrasensitive Solution-Cast Quantum Dot Photodetectors. *Nature* **2006**, *442* (7099), 180−183.

(4) Clifford, J. P.; Konstantatos, G.; Johnston, K. W.; Hoogland, S.; Levina, L.; Sargent, E. H. Fast, Sensitive and Spectrally Tuneable Colloidal-Quantum-Dot Photodetectors. *Nat. Nanotechnol.* **2009**, *4* (1), 40−44.

(5) Carey, G. H.; Kramer, I. J.; Kanjanaboos, P.; Moreno-Bautista, G.; Voznyy, O.; Rollny, L.; Tang, J. A.; Hoogland, S.; Sargent, E. H. Electronically Active Impurities in Colloidal Quantum Dot Solids. *ACS Nano* **2014**, *8*, 11763−11769.

(6) Chuang, C.-H. M.; Brown, P. R.; Bulović, V.; Bawendi, M. G. Improved Performance and Stability in Quantum Dot Solar Cells through Band Alignment Engineering. *Nat. Mater.* **2014**, *13*, 796−801.

(7) Liu, M.; Voznyy, O.; Sabatini, R.; García De Arquer, F. P.; Munir, R.; Balawi, A. H.; Lan, X.; Fan, F.; Walters, G.; Kirmani, A. R.; et al. Hybrid Organic-Inorganic Inks Flatten the Energy Landscape in Colloidal Quantum Dot Solids. *Nat. Mater.* **2017**, *16* (2), 258−263.

(8) Carey, G. H.; Abdelhady, A. L.; Ning, Z.; Thon, S. M.; Bakr, O. M.; Sargent, E. H. Colloidal Quantum Dot Solar Cells. *Chem. Rev.* **2015**, *115*, 12732−12763.

(9) Kagan, C.; Murray, C.; Nirmal, M.; Bawendi, M. Electronic Energy Transfer in CdSe Quantum Dot Solids. *Phys. Rev. Lett.* **1996**, *76* (9), 1517−1520.

(10) Balazs, D. M.; Matysiak, B. M.; Momand, J.; Shulga, A. G.; Ibáñez, M.; Kovalenko, M. V.; Kooi, B. J.; Loi, M. A. Electron Mobility of 24 Cm 2 V − 1 s − 1 in PbSe Colloidal-Quantum-Dot Superlattices. *Adv. Mater.* **2018**, *30* (38), 1802265.

(11) Balazs, D. M.; Loi, M. A. Lead-Chalcogenide Colloidal-Quantum-Dot Solids: Novel Assembly Methods, Electronic Structure Control, and Application Prospects. *Adv. Mater.* **2018**, *30* (33), 1800082.

(12) Liu, Y.; Gibbs, M.; Puthussery, J.; Gaik, S.; Ihly, R.; Hillhouse, H. W.; Law, M. Dependence of Carrier Mobility on Nanocrystal Size and Ligand Length in PbSe Nanocrystal Solids. *Nano Lett.* **2010**, *10* (5), 1960−1969.

(13) Brown, P. R.; Kim, D.; Lunt, R. R.; Zhao, N.; Bawendi, M. G.; Grossman, J. C.; Bulović, V. Energy Level Modification in Lead Sulfide Quantum Dot Thin Films through Ligand Exchange. *ACS Nano* **2014**, *8*, 5863−5872.

(14) Giansante, C.; Infante, I.; Fabiano, E.; Grisorio, R.; Suranna, G. P.; Gigli, G. Darker-than-Black" PbS Quantum Dots: Enhancing Optical Absorption of Colloidal Semiconductor Nanocrystals *via* Short Conjugated Ligands. *J. Am. Chem. Soc.* **2015**, *137*, 1875−1886.

(15) Li, H.; Zhitomirsky, D.; Dave, S.; Grossman, J. C. Toward the Ultimate Limit of Connectivity in Quantum Dots with High Mobility and Clean Gaps. *ACS Nano* **2016**, *10*, 606.

(16) Hughes, B. K.; Blackburn, J. L.; Kroupa, D.; Shabaev, A.; Erwin, S. C.; Efros, A. L.; Nozik, A. J.; Luther, J. M.; Beard, M. C. Synthesis and Spectroscopy of Pbse Fused Quantum-Dot Dimers. *J. Am. Chem. Soc.* **2014**, *136* (12), 4670−4679.

(17) Baumgardner, W. J.; Whitham, K.; Hanrath, T. Confined-but-Connected Quantum Solids via Controlled Ligand Displacement. *Nano Lett.* **2013**, *13* (7), 3225−3231.

(18) Hanrath, T.; Veldman, D.; Choi, J. J.; Christova, C. G.; Wienk, M. M.; Janssen, R. A. J. PbSe Nanocrystal Network Formation during Pyridine Ligand Displacement. *ACS Appl. Mater. Interfaces* **2009**, *1* (2), 244−250.

(19) Gilmore, R. H.; Lee, E. M. Y.; Weidman, M. C.; Willard, A. P.; Tisdale, W. A. Charge Carrier Hopping Dynamics in Homogeneously

DOI: 10.1021/acs.jpclett.9b01282
J. Phys. Chem. Lett. 2019, 10, 3756−3762

Broadened PbS Quantum Dot Solids. *Nano Lett.* **2017**, *17* (2), 893−901.
(20) Weidman, M. C.; Beck, M. E.; Hoffman, R. S.; Prins, F.; Tisdale, W. A. Monodisperse, Air-Stable PbS Nanocrystals *via* Precursor Stoichiometry Control. *ACS Nano* **2014**, *8*, 6363−6371.
(21) Weidman, M. C.; Smilgies, D.-M.; Tisdale, W. A. Kinetics of the Self-Assembly of Nanocrystal Superlattices Measured by Real-Time in Situ X-Ray Scattering. *Nat. Mater.* **2016**, *15*, 775−781.
(22) Evers, W. H.; Goris, B.; Bals, S.; Casavola, M.; De Graaf, J.; van Roij, R.; Dijkstra, M.; Vanmaekelbergh, D. Low-Dimensional Semiconductor Superlattices Formed by Geometric Control over Nanocrystal Attachment. *Nano Lett.* **2013**, *13* (6), 2317−2323.
(23) Kovalenko, M. V.; Manna, L.; Cabot, A.; Hens, Z.; Talapin, D. V.; Kagan, C. R.; Klimov, V. I.; Rogach, A. L.; Reiss, P.; Milliron, D. J.; et al. Prospects of Nanoscience with Nanocrystals. *ACS Nano* **2015**, *9* (2), 1012−1057.
(24) Wu, Y.; Li, S.; Gogotsi, N.; Zhao, T.; Fleury, B.; Kagan, C. R.; Murray, C. B.; Baxter, J. B. Directional Carrier Transfer in Strongly Coupled Binary Nanocrystal Superlattice Films Formed by Assembly and in Situ Ligand Exchange at a Liquid-Air Interface. *J. Phys. Chem. C* **2017**, *121*, 4146−4157.
(25) Kalesaki, E.; Evers, W. H.; Allan, G.; Vanmaekelbergh, D.; Delerue, C. Electronic Structure of Atomically Coherent Square Semiconductor Superlattices with Dimensionality below Two. *Phys. Rev. B: Condens. Matter Mater. Phys.* **2013**, *88* (11), 115431.
(26) Kalesaki, E.; Delerue, C.; Morais Smith, C.; Beugeling, W.; Allan, G.; Vanmaekelbergh, D. Dirac Cones, Topological Edge States, and Nontrivial Flat Bands in Two-Dimensional Semiconductors with a Honeycomb Nanogeometry. *Phys. Rev. X* **2014**, *4* (1), 011010.
(27) Yu, D.; Wang, C.; Wehrenberg, B. L.; Guyot-Sionnest, P. Variable Range Hopping Conduction in Semiconductor Nanocrystal Solids. *Phys. Rev. Lett.* **2004**, *92* (21), 216802.
(28) Chu, I. H.; Radulaski, M.; Vukmirovic, N.; Cheng, H. P.; Wang, L. W. Charge Transport in a Quantum Dot Supercrystal. *J. Phys. Chem. C* **2011**, *115* (43), 21409−21415.
(29) Whitham, K.; Yang, J.; Savitzky, B. H.; Kourkoutis, L. F.; Wise, F.; Hanrath, T. Charge Transport and Localization in Atomically Coherent Quantum Dot Solids. *Nat. Mater.* **2016**, *15*, 557−563.
(30) Choi, J. H.; Fafarman, A. T.; Oh, S. J.; Ko, D. K.; Kim, D. K.; Diroll, B. T.; Muramoto, S.; Gillen, J. G.; Murray, C. B.; Kagan, C. R. Bandlike Transport in Strongly Coupled and Doped Quantum Dot Solids: A Route to High-Performance Thin-Film Electronics. *Nano Lett.* **2012**, *12* (5), 2631−2638.
(31) Lee, J.-S.; Kovalenko, M. V.; Huang, J.; Chung, D. S.; Talapin, D. V. Band-like Transport, High Electron Mobility and High Photoconductivity in All-Inorganic Nanocrystal Arrays. *Nat. Nanotechnol.* **2011**, *6* (6), 348−352.
(32) Evers, W. H.; Schins, J. M.; Aerts, M.; Kulkarni, A.; Capiod, P.; Berthe, M.; Grandidier, B.; Delerue, C.; van der Zant, H. S. J.; van Overbeek, C.; Peters, J. L.; Vanmaekelbergh, D.; Siebbeles, L. D. A. High Charge Mobility in Two-Dimensional Percolative Networks of PbSe Quantum Dots Connected by Atomic Bonds. *Nat. Commun.* **2015**, *6*, 8195.
(33) Liu, Y.; Kim, D.; Morris, O. P.; Zhitomirsky, D.; Grossman, J. C. On the Origins of the Stokes Shift in PbS Quantum Dots: Impact of Polydispersity, Ligands and Defects. *ACS Nano* **2018**, *12*, 2838−2845.
(34) An, J. M.; Franceschetti, A.; Dudiy, S. V.; Zunger, A. The Peculiar Electronic Structure of PbSe Quantum Dots. *Nano Lett.* **2006**, *6*, 2728−2735.
(35) Bardeen, J.; Shockley, W. Deformation Potentials and Mobilities in Non-Polar Crystals. *Phys. Rev.* **1950**, *80* (1), 72−80.
(36) Wei, S. H.; Zunger, A. Electronic and Structural Anomalies in Lead Chalcogenides. *Phys. Rev. B: Condens. Matter Mater. Phys.* **1997**, *55*, 13605−13610.
(37) Zhang, Y.; Ke, X.; Chen, C.; Yang, J.; Kent, P. R. C. Thermodynamic Properties of PbTe, PbSe, and PbS: First-Principles Study. *Phys. Rev. B: Condens. Matter Mater. Phys.* **2009**, *80* (2), 024304.
(38) Hummer, K.; Grüneis, A.; Kresse, G. Structural and Electronic Properties of Lead Chalcogenides from First Principles. *Phys. Rev. B: Condens. Matter Mater. Phys.* **2007**, *75* (19), 195211.
(39) Gibbs, Z. M.; Ricci, F.; Li, G.; Zhu, H.; Persson, K.; Ceder, G.; Hautier, G.; Jain, A.; Snyder, G. J. Effective Mass and Fermi Surface Complexity Factor from Ab Initio Band Structure Calculations. *npj Comput. Mater.* **2017**, *3* (1), 8.
(40) Ravich, Y. I.; Efimova, B. A.; Tamarchenko, V. I. Scattering of Current Carriers and Transport Phenomena in Lead Chalcogenides II. Experiment. *Phys. Status Solidi B* **1971**, *43* (2), 453−469.
(41) Zherebetskyy, D.; Zhang, Y.; Salmeron, M.; Wang, L.-W. Tolerance of Intrinsic Defects in PbS Quantum Dots. *J. Phys. Chem. Lett.* **2015**, *6*, 4711−4716.
(42) Tang, J.; Kemp, K. W.; Hoogland, S.; Jeong, K. S.; Liu, H.; Levina, L.; Furukawa, M.; Wang, X.; Debnath, R.; Cha, D.; et al. Colloidal-Quantum-Dot Photovoltaics Using Atomic-Ligand Passivation. *Nat. Mater.* **2011**, *10*, 765−771.
(43) Ning, Z.; Zhitomirsky, D.; Adinolfi, V.; Sutherland, B.; Xu, J.; Voznyy, O.; Maraghechi, P.; Lan, X.; Hoogland, S.; Ren, Y.; et al. Graded Doping for Enhanced Colloidal Quantum Dot Photovoltaics. *Adv. Mater.* **2013**, *25* (12), 1719−1723.
(44) Osedach, T. P.; Zhao, N.; Andrew, T. L.; Brown, P. R.; Wanger, D. D.; Strasfeld, D. B.; Chang, L. Y.; Bawendi, M. G.; Bulovic, V. Bias-Stress Effect in 1,2-Ethanedithiol-Treated PbS Quantum Dot Field-Effect Transistors. *ACS Nano* **2012**, *6* (4), 3121−3127.
(45) Wanger, D. D.; Correa, R. E.; Dauler, E. a.; Bawendi, M. G. The Dominant Role of Exciton Quenching in PbS Quantum-Dot-Based Photovoltaic Devices. *Nano Lett.* **2013**, *13* (12), 5907−5912.
(46) Allgaier, R. S.; Scanlon, W. W. Mobility of Electrons and Holes in PbS, PbSe, and PbTe between Room Temperature and 4.2 K. *Phys. Rev.* **1958**, *111* (4), 1029−1037.
(47) Fang, C.; Van Huis, M. a.; Vanmaekelbergh, D.; Zandbergen, H. W. Energetics of Polar and Nonpolar Facets of PbSe Nanocrystals from Theory and Experiment. *ACS Nano* **2010**, *4* (1), 211−218.
(48) Choi, H.; Ko, J.; Kim, Y.; Jeong, S. Steric Hindrance Driven Shape Transition in PbS Quantum Dots: Understanding Size-Dependent Stability. *J. Am. Chem. Soc.* **2013**, *135*, 5278−5281.
(49) Zherebetskyy, D.; Scheele, M.; Zhang, Y.; Bronstein, N.; Thompson, C.; Britt, D.; Salmeron, M.; Alivisatos, P.; Wang, L.-W. Hydroxylation of the Surface of PbS Nanocrystals Passivated with Oleic Acid. *Science (Washington, DC, U. S.)* **2014**, *344* (80), 1380−1384.
(50) Kang, M. S.; Sahu, A.; Norris, D. J.; Frisbie, C. D. Size-Dependent Electrical Transport in CdSe Nanocrystal Thin Films. *Nano Lett.* **2010**, *10* (9), 3727−3732.
(51) Scheele, M.; Engel, J. H.; Ferry, V. E.; Hanifi, D.; Liu, Y.; Alivisatos, A. P. Nonmonotonic Size Dependence in the Hole Mobility of Methoxide-Stabilized PbSe Quantum Dot Solids. *ACS Nano* **2013**, *7* (8), 6774−6781.
(52) Lee, J.; Choi, O.; Sim, E. Nonmonotonic Size-Dependent Carrier Mobility in PbSe Nanocrystal Arrays. *J. Phys. Chem. Lett.* **2012**, *3* (6), 714−719.
(53) Boneschanscher, M. P.; Evers, W. H.; Geuchies, J. J.; Altantzis, T.; Goris, B.; Rabouw, F. T.; van Rossum, S. a. P.; van der Zant, H. S. J.; Siebbeles, L. D. a.; Van Tendeloo, G.; Swart, I.; Hilhorst, J.; Petukhov, A. V.; Bals, S.; Vanmaekelbergh, D. Long-Range Orientation and Atomic Attachment of Nanocrystals in 2D Honeycomb Superlattices. *Science* **2014**, *344* (6190), 1377−1380.
(54) Kresse, G.; Furthmüller, J. Efficient Iterative Schemes for *Ab Initio* Total-Energy Calculations Using a Plane-Wave Basis Set. *Phys. Rev. B: Condens. Matter Mater. Phys.* **1996**, *54*, 11169−11186.
(55) Kresse, G.; Furthmüller, J. Efficiency of Ab-Initio Total Energy Calculations for Metals and Semiconductors Using a Plane-Wave Basis Set. *Comput. Mater. Sci.* **1996**, *6*, 15−50.
(56) Kresse, G.; Joubert, D. From Ultrasoft Pseudopotentials to the Projector Augmented-Wave Method. *Phys. Rev. B: Condens. Matter Mater. Phys.* **1999**, *59*, 1758−1775.
(57) Perdew, J. P.; Burke, K.; Ernzerhof, M. Generalized Gradient Approximation Made Simple. *Phys. Rev. Lett.* **1996**, *77*, 3865−3868.

DOI: 10.1021/acs.jpclett.9b01282
J. Phys. Chem. Lett. 2019, 10, 3756−3762

(58) Madsen, G. K. H.; Singh, D. J. BoltzTraP. A Code for Calculating Band-Structure Dependent Quantities. *Comput. Phys. Commun.* **2006**, *175* (1), 67−71.

DOI: 10.1021/acs.jpclett.9b01282
J. Phys. Chem. Lett. 2019, 10, 3756−3762